

RESEARCH

Open Access



Investigation and modulation of interleukin-6 following subarachnoid hemorrhage: targeting inflammatory activation for cerebral vasospasm

Brandon Lucke-Wold^{1*}, William Dodd¹, Kartik Motwani¹, Koji Hosaka¹, Dimitri Laurent¹, Melanie Martinez¹, Victoria Dugan², Nohra Chalouhi¹, Noelle Lucke-Wold³, Arnav Barpujari¹, Christina von Roemeling¹, Chenglong Li⁴, Richard D. Johnson² and Brian Hoh¹

Abstract

Background: Cerebral vasospasm (CV) can contribute to significant morbidity in subarachnoid hemorrhage (SAH) patients. A key unknown is how CV induction is triggered following SAH.

Methods: Human aneurysmal blood and cerebral spinal fluid were collected for evaluation. To confirm mechanism, c57/bl6 wild type and c57/bl6 IL-6 female knockout (KO) mice were utilized with groups: saline injected, SAH, SAH + IL-6 blockade, SAH IL-6 KO, SAH IL-6 KO + IL-6 administration, SAH + p-STAT3 inhibition. Dual-labeled microglia/myeloid mice were used to show myeloid diapedesis. For SAH, 50 μ m blood was collected from tail puncture and administered into basal cisterns. IL-6 blockade was given at various time points. Various markers of neuroinflammation were measured with western blot and immunohistochemistry. Cerebral blood flow was also measured. Vasospasm was measured via cardiac injection of India ink/gelatin. Turning test and Garcia's modified SAH score were utilized. $P < 0.05$ was considered significant.

Results: IL-6 expression peaked 3 days following SAH ($p < 0.05$). Human IL-6 was increased in aneurysmal blood ($p < 0.05$) and in cerebral spinal fluid ($p < 0.01$). Receptor upregulation was periventricular and perivascular. Microglia activation following SAH resulted in increased caveolin 3 and myeloid diapedesis. A significant increase in BBB markers endothelin 1 and occludin was noted following SAH, but reduced with IL-6 blockade ($p < 0.01$). CV occurred 5 days post-SAH, but was absent in IL-6 KO mice and mitigated with IL-6 blockade ($p < 0.05$). IL-6 blockade, and IL-6 KO mitigated effects of SAH on cerebral blood flow ($p < 0.05$). SAH mice had impaired performance on turn test and poor modified Garcia scores compared to saline and IL-6 blockade. A distinct microglia phenotype was noted day 5 in the SAH group (overlap coefficients $r = 0.96$ and $r = 0.94$) for Arg1 and iNOS, which was altered by IL-6 blockade. Day 7, a significant increase in toll-like receptor 4 and Stat3 was noted. This was mitigated by IL-6 blockade and IL-6 KO, which also reduced Caspase 3 ($p < 0.05$). To confirm the mechanism, we developed a p-STAT3 inhibitor that targets the IL-6 pathway and this reduced NF κ B, TLR4, and nitrotyrosine ($p < 0.001$). Ventricular dilation and increased Tunel positivity was noted day 9, but resolved by IL-6 blockade ($p < 0.05$).

*Correspondence: Brandon.Lucke-Wold@neurosurgery.ufl.edu

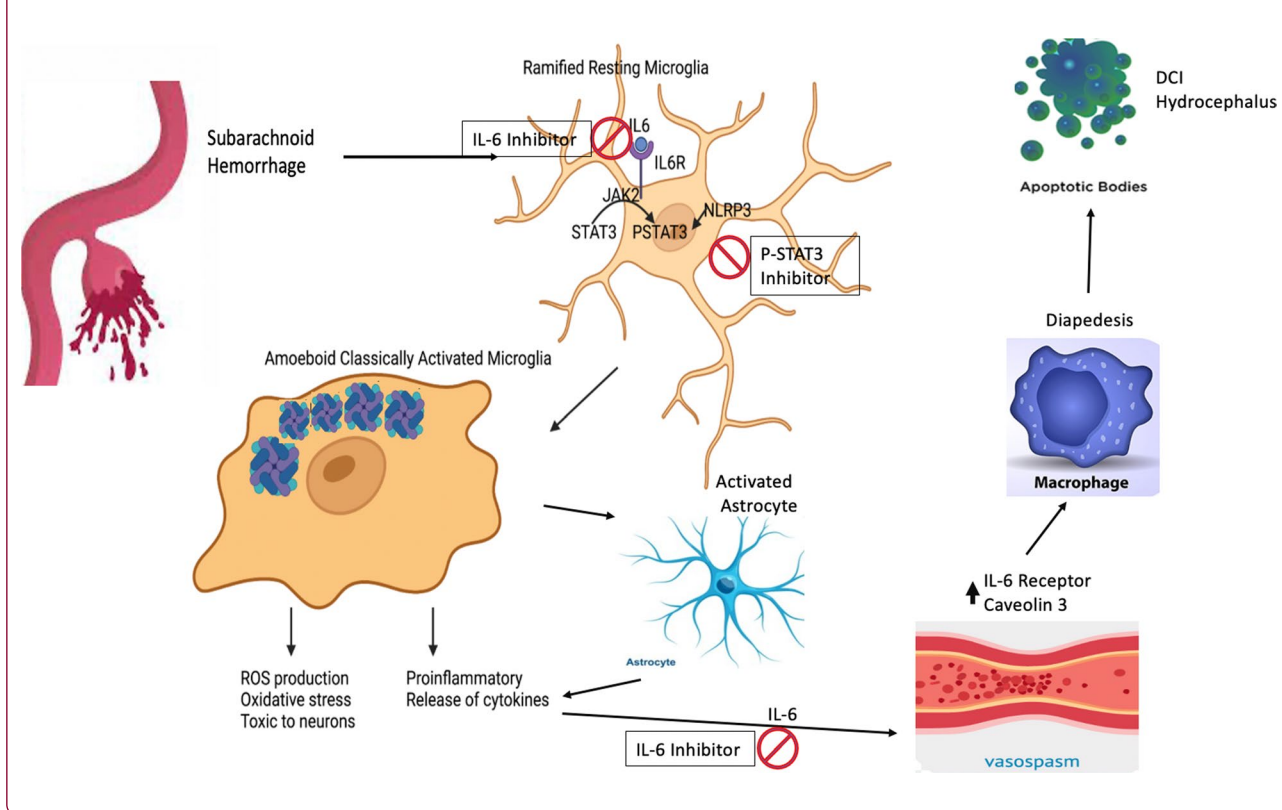
¹ Department of Neurosurgery, University of Florida, Gainesville, FL, USA
Full list of author information is available at the end of the article



Conclusion: Correlation between IL-6 and CV has been well documented. We show that a mechanistic connection exists via the p-STAT3 pathway, and IL-6 blockade provides benefit in reducing CV and its consequences mediated by myeloid cell origin diapedesis.

Keywords: Interleukin-6, Subarachnoid hemorrhage, Vasospasm, Microglia activation, p-STAT3

Graphical abstract



Introduction

Subarachnoid hemorrhage (SAH) is associated with high morbidity and mortality. 70% of SAH patients develop imaging characteristics of vasospasm and 30% become clinically symptomatic [1]. An increase in interleukin-6 (IL-6) has been shown to shortly precede vasospasm in both clinical and pre-clinical studies [2]. Underlying mechanisms for why this occurs have been poorly elucidated. Emerging interest has led several groups to review the clinical and pre-clinical literature regarding IL-6’s role in vasospasm development [3]. The temporal relationship is unmistakable. The spike in IL-6 in both pre-clinical and clinical specimens occur within a 3- to 5-day window and can remain elevated for several days thereafter [4]. The few pre-clinical studies targeting IL-6 following SAH have found reduced cell death and decreased evidence of delayed cerebral ischemia (DCI) [5].

In our recent review, we postulate the important role that the IL-6 pathway plays in the downstream

consequences of SAH [6]. IL-6 release has been closely tied to reactive astrocytes that are critical in blood product breakdown following SAH [7]. Once IL-6 is released, it initiates a robust perivascular inflammatory response [8]. Recent evidence shows that part of the inflammatory response involves microglia activation, and in particular a desensitized amoeboid phenotype that may have a variety of morphologies [9]. These activated microglia release cytokines such as IL-6 that contribute to peripheral macrophage diapedesis. This paper looks at some of the downstream modulation on neuroinflammation with regard to targeting IL-6. Activated microglia express toll-like receptor 4 and can initiate the STAT3 pathway, which has been linked to DCI via inflammatory storming from macrophage infiltration. The pathway initiates a pro-inflammatory positive feedback loop for IL-6, which allows ongoing activity. To mechanistically confirm the role of the IL-6 pathway, we selectively targeted p-STAT3 with a custom

inhibitor. The activated pathway converts traditional senescent microglia into a pro-inflammatory state that in conjunction with macrophage diapedesis causes cortical neuronal apoptosis, micro-destruction of the blood brain barrier (BBB), and hydrocephalus [10]. In this paper, our objective was to critically investigate the mechanistic IL-6 pathway with a focus on the induction of vasospasm via the initiation of this inflammatory pathway and its downstream STAT3 cascade. Utilizing both transgenic knock outs, dual-labeled microglia/myeloid mice, a focused IL-6 inhibitor, and a custom p-STAT3 inhibitor we tease apart a contributory mechanism to vasospasm.

Methods

Human samples

Human blood and cerebral spinal fluid collection from aneurysm patients was approved by University of Florida Institutional Review Board (IRB202002035). Patient data were deidentified for storage into the database. Four female patient samples were collected from ruptured cerebral aneurysm blood at time of endovascular treatment of aneurysm. 6 ml of blood was collected from microcatheter positioned adjacent to ruptured aneurysm (representative of cerebral circulation blood). 6 ml of blood was collected from sheath in the wrist or groin (radial or femoral blood representative of systemic circulation). Blood was stored on ice and immediately spun in centrifuge post-procedure for processing. Serum was collected and stored in -80°C freezer until use for western blot. These four patients had anterior circulation aneurysms that were coiled, Hunt and Hess score of 2 or 3 at time of presentation, and a modified Fisher score of 3 or 4. All these patients had an external ventricular drain placed as well with cerebrospinal fluid collected at time of aneurysm coiling. Patients were excluded if no external ventricular drain was placed. The cerebrospinal fluid was compared to normal controls (pseudotumor patients) who had cerebrospinal fluid collected via lumbar puncture during diagnostic workup (IRB202200182). All cerebrospinal fluid samples were stored at -80°C prior to processing via ELISA. Similarly, aneurysm peripheral blood was compared to control peripheral blood samples via ELISA.

Animals

All animal experiments were performed in accordance with the Animal Research: Reporting of In Vivo Experiments guidelines and were approved and supported by the University of Florida Institutional Animal Care and Use Committee. All animals were either C57BL/6 wild type, IL-6 knockout mice bred in C57BL/6 background, or CCR2-/CXCR1 mice graciously donated by the

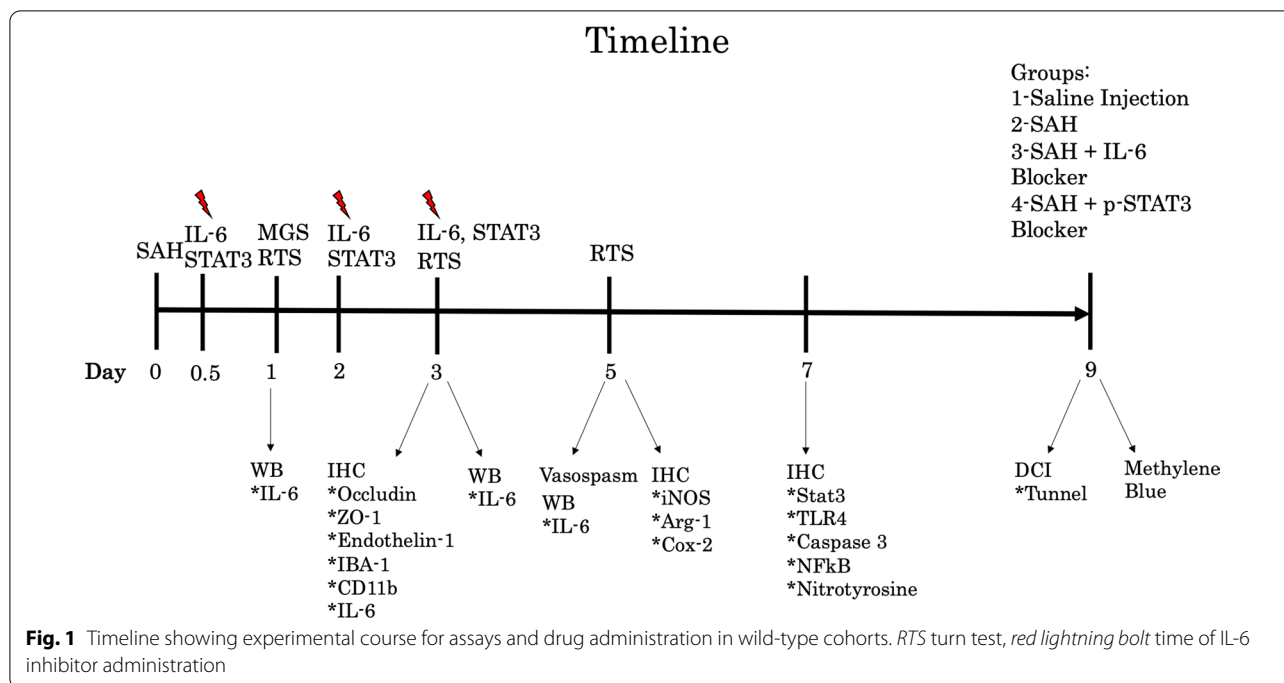
Harrison Laboratory. Mice were between 12- to 15-week-old females. They were housed with ad libitum food and water and 12-h light/dark cycling. All wild-type mice were received from Charles River Labs (Wilmington, MA). IL-6 knockout mice were received from The Jackson Laboratory (Bar Harbor, ME). Cages were randomly assigned to groups to make experimental groups even prior to surgical intervention. Experimental timeline is outlined in Fig. 1.

Subarachnoid hemorrhage

The SAH model utilized modified autologous blood injection to basal cisterns adjacent to right anterior circulation [11]. Briefly, mice were anesthetized with 10 mg/kg xylazine and 100 mg/kg ketamine prior to shaving/cleaning the scalp. The tail was prepped, shaved, and cleaned. The mouse's head was fixed to the stereotaxic frame and body temperature maintained at 37°C using a heating pad. The scalp was incised along the sagittal suture from bregma to the nasal bone. The skin was reflected and held in place by retraction. The burr hole was positioned 5.0 mm rostral to bregma and 0.5 mm right of midline. Next, 150 μL of arterial blood was drawn from the tail artery. 50 μL of blood was drawn up into a Hamilton syringe. 50 μL was chosen in accordance with the reported range for animal weights used in this study (19–24 g). 30 μL –100 μL has been reported in the literature based on a recent systematic review with the primary adjustment being according to animal weight [12]. The syringe needle was passed at a 30° caudal angle until it reached the skull base. The syringe was left in place and blood was manually injected at a rate of 10 $\mu\text{L}/\text{min}$. The mouse's respiratory rate was closely monitored. Sham procedure was identical to the above except no tail blood was collected, but instead saline injected. Once the needle was removed, the skin flap was sutured with 5-0 ethilon suture. The mice were administered buprenorphine as an analgesic and placed on a warmer until recovered from anesthesia.

Vasospasm

Ten mice per group were utilized. Five days post-SAH, mice were deeply anesthetized with ketamine and xylazine. Cardiac catheterization was performed, and perfusion was done with 5 ml PBS followed by 15 ml of 4% paraformaldehyde. 20% India ink was dissolved in 5% gelatin and heated. 2 ml of India ink solution was perfused at a rate of 15 ml/min after the administration of paraformaldehyde. The mouse carcass was then stored at 4°C for 6 h to allow hardening. Brains were imaged and the ipsilateral anterior cerebral and middle cerebral artery were captured. The narrowest diameter within the M1 segment was measured as a ratio against average A1 segment diameter. Mice with bifurcated or aplastic vessels



were excluded. The ratio is a reliable measure of vasospasm as previously reported [11].

Cerebral blood flow

Four mice per group were utilized. Cerebral blood flow was measured with a laser speckle perfusion imager at 48 h after SAH. The protocol was like that previously described [13]. Briefly, mice were anesthetized, scalp prepped, and skin removed to reveal skull surface. Sufficient readings were able to be achieved without bone flap removal. The speckle perfusion imager was placed ~10 cm above the skull and leveled to a baseline value of 100 (Pericam PSI System, PeriMed). Recordings were done for 2 min per animal. A color-coded image was displayed and converted into numerical scoring based on computer algorithm (PIMsoft, PeriMed, Stockholm, Sweden). Average perfusion per animal was documented and an imaging voxel with a calculated mean of 9.7 was used to measure bilateral MCA territory perfusion. A ratio of right to left MCA perfusion was calculated for each animal to allow reliable comparisons between groups and to control for variance in baseline blood pressure differences.

Pharmaceutical dosing

To neutralize IL-6, intraperitoneal injection of IL-6 blocking antibody (Bio X Cell, Lebanon, NH) was administered at a concentration of 10 µg/g at 12 h post-blood injection, 48 h post-blood injection, and 72 h post-blood injection. Dosing was chosen based on prior experimental efficacy

with C57BL/6 mice [14]. For the knockout mice, to confirm effect of IL-6, endogenous administration of IL-6 was performed 6 h prior to blood injection and then daily until time of euthanasia. Recombinant IL-6 (Peprotech, Inc., Rocky Hill, NJ, USA) was administered at 3.2 ng/g per day based on prior protocols [15]. To confirm pathway specificity, we worked with our medicinal chemist colleague to develop a custom p-STAT3 inhibitor that selectively crosses the blood brain barrier. LLL12B was administered at 5 mg/kg dosing 1, 2, and 3 days after SAH.

Neurologic evaluation

Eight mice per group were utilized. Mice were observed and scored based on the modified Garcia score and corner test. The modified Garcia score consists of six tests involving assessment of whisker stimulation, climbing, body proprioception, forepaw outstretching, spontaneous activity, and movement of four limbs [16]. For the corner test, two 20-cm boards were adjoined at 30° and placed on a clean testing environment. Mice were acclimatized to the apparatus for 10 min prior to SAH or saline administration. The mice were tested post-SAH as previously described [17]. Briefly, the mouse was placed directly in the middle of the two boards with nose facing the angle. The mouse entered deep into the corner and would rear to turn. The turn was recorded as either right or left. 10 total turns were recorded for each animal per day.

Western blot and ELISA

Six mice per group were utilized for protein collection from either blood or right frontal cortex as previously described [18]. Briefly, for blood collection six mice per group were anesthetized and 2 ml of blood collected via cardiac catheterization. The blood was spun at 3000 rpm for 15 min, and serum collected for protein analysis. For brain tissue collection, six mice per group were anesthetized and perfused with 10 ml of ice-cold phosphate buffered saline (PBS). Rapid decapitation with careful removal of brain and placement on brain matrix (Harvard Apparatus, Holliston, MA) was performed. The right frontal cortex was sectioned and snap-frozen in liquid nitrogen. Once frozen, it was homogenized with a Dounce homogenizer and agitated in radio-immunoprecipitation assay (RIPA) buffer for 90 min. Samples were centrifuged, supernatant collected, and protein quantified via the Bradford assay. Samples were stored in -20°C . 35 μg of protein was separated on 4–15% Tris–glycine gels at 90 V for a total of 60 min. The protein was then transferred to nitrocellulose membranes. Membranes were blocked with 5% skim milk in Tris-buffered saline tween 20 (TBS-T) for 1 h at room temperature. The blocking solution was washed off with rinses of TBS-T and membrane probed with primary antibodies overnight at room temperature. Primary antibodies utilized were rabbit anti-mouse IL-6 28 kDa (1:1000, Abcam, Branford, CT), rat anti-mouse β -actin 42 kDa (1:5000, Cell Signaling, Danvers, MA), and rabbit anti-mouse p-STAT3 88 kDa (1:1000, Cell Signaling, Danvers, MA). The membranes were then washed with TBS-T and incubated with HRP-conjugated secondary antibody (1:2000, Abcam, Branford, CT) for 1 h at room temperature. Membranes were washed and incubated in luminol-peroxide solution (Santa Cruz Biotechnology, Dallas, TX) for 1 min and taken to the dark room. Films were developed, and densitometry performed with ImageJ software. Band densities for protein of interest were normalized to β -actin. ELISA was done according to manufacturer instructions per kit (Abcam, Waltham, MA).

Immunohistochemistry

Six mice per group were utilized. Mice were anesthetized and cardiac perfused with PBS at a rate of 5 ml/min. Brains were removed, placed in plastic cassette with OCT, and submerged in -65°C isopentane. The blocks were stored at -80°C . On day of sectioning, the OCT blocks were mounted for the Leica CM3050S cryostat (Leica Microsystems) and sliced at a thickness of 14 μm . Slices were collected on a mounted glass slide. The staining protocol was similar to that previously published [19]. After initial serial washes, brain slices were incubated overnight with primary antibodies according to

manufacturer recommended dilutions. Antibodies used: Endothelin-1, ZO-1, Occludin, GFAP, p-STAT3, Arg1, Cox2, NF κ B, and caspase 3 (Cell Signaling, Danvers, MA), IL-6R, IL-6, iNOS, Caveolin 3 (Abcam, Branford, CT), IBA-1, CD11B (Invitrogen, Waltham, MA), nitrotyrosine (Millipore Sigma, Burlington, MA), and TLR-4 (Proteintech, Rosemont, IL). The slides were then rinsed, and Alexa Fluor secondary antibodies were applied to the slides for 3 h. The slide was rinsed and Vectashield 4',6-diamidino-2-phenylindole (DAPI) nuclear counterstain was applied (Vector, Burlingame, CA).

Right frontal and periventricular regions were examined. Ten slides per animal were prepared. Olympus IX71 fluorescent microscope (Olympus America, Center Valley, PA) was used. For fluorescent assays, total corrected cell fluorescent protocol was utilized as previously described [18]. For cellular morphology assays, total number of cells per high power field were compared as previously described by blinded observer [20]. This method was utilized for NeuN-stained slides with Tunel assay according to manufacturer instructions (Abcam, Cambridge, MA). For co-localization assays, the Just Another Co-localization Plugin from ImageJ was utilized with Costes correction [21]. The vessel disruption percentage was calculated as percentage of luminal irregularity by methods previously described [22]. Ventricle post-mortem size assessment was done with methylene blue staining according to methods previously described [23]. Clarity analysis was done according to standard protocol [24].

Statistical analysis

Western blot, Tunel, immunohistochemistry, vasospasm, and behavioral assays were evaluated with one-way ANOVA with Tukey post hoc comparison to determine differences between groups. For comparison between two groups, a Student's *t*-test was performed. Power calculations were completed for vasospasm with $\alpha=0.05$, $\beta=0.2$, and minimum difference expected between groups of 20%. Overlap coefficient was determined with ImageJ software and the Just Another Co-localization Plug In. GraphPad Prismv8.0 (GraphPad Software, San Diego, CA) was utilized for statistical analysis with $p<0.05$ considered significant.

Results

IL-6 peaks on day 3 and has periventricular and perivascular release

IL-6 was measured in peripheral blood on Day 1, 3, and 5 following SAH. No significant difference was seen on day 1 post-SAH with a mean difference of 0.04 between saline and SAH ($t=0.79$, $p=0.46$). A significant increase was seen on day 3 post-SAH with a mean difference 1.75

between saline vs. SAH ($t=2.91, p=0.027$). A continued peak was seen on day 5 post-SAH with a mean difference 0.28 between saline vs. SAH ($t=3.33, p=0.016$) (Fig. 2A). IL-6 was increased in perianeurysmal blood compared to sheath blood for human samples at time of aneurysm treatment with mean difference 0.269 ($t=3.001, p=0.024$) (Fig. 2B). IL-6 receptor upregulation within the brain was seen in a periventricular distribution (Fig. 2C). IL-6 measurements within the brain were upregulated near the periventricular space (Fig. 2D). When co-localized with astrocytic marker GFAP and endothelial marker CD31, it was noted that the IL-6 expression was within the skull base microvasculature adjacent to astrocyte podocytes (Fig. 2E).

IL-6 increases in CSF compared to control with novel target for STAT3 modulation

CSF was compared between SAH patients and healthy controls. Average pg/ml of IL-6 in control CSF was 5 compared to 1686 for SAH patient CSF ($t=3.29, p<0.01$) (Fig. 3A). No significant difference was seen in IL-6 levels between peripheral IV serum samples between groups.

Average pg/ml of IL-6 in control peripheral serum was 5 compared to 8 for the SAH patients ($t=0.61, p=0.55$) (Fig. 3B). The CNS-specific surge in IL-6 prompted the development of a focused small molecule inhibitor LLL12b that could cross the BBB and selectively target inflammation and oxidative stress. Chemical formulation is outlined in Fig. 3C.

IL-6 blockade mitigates blood brain barrier disruption and microglia activation

Post-SAH day 3 endothelin-1 staining was done to look at luminal irregularity in microvasculature of right MCA region. A significant difference was seen between groups ($F(2,9)=34.48, p<0.001$). The mean difference was 2.53 between saline and SAH ($q=11.7, p<0.001$). This effect was mitigated with IL-6 blockade with mean difference 1.467 between SAH vs. SAH+IL-6 block ($q=6.77, p=0.003$) (Fig. 4A). Microglia recruitment to the perivascular space was significantly different between groups as measured with CD11b and IBA-1 ($F(2,27)=62.79, p<0.001$). A mean difference of 0.44 was seen between saline vs. SAH ($q=12.47, p<0.001$).

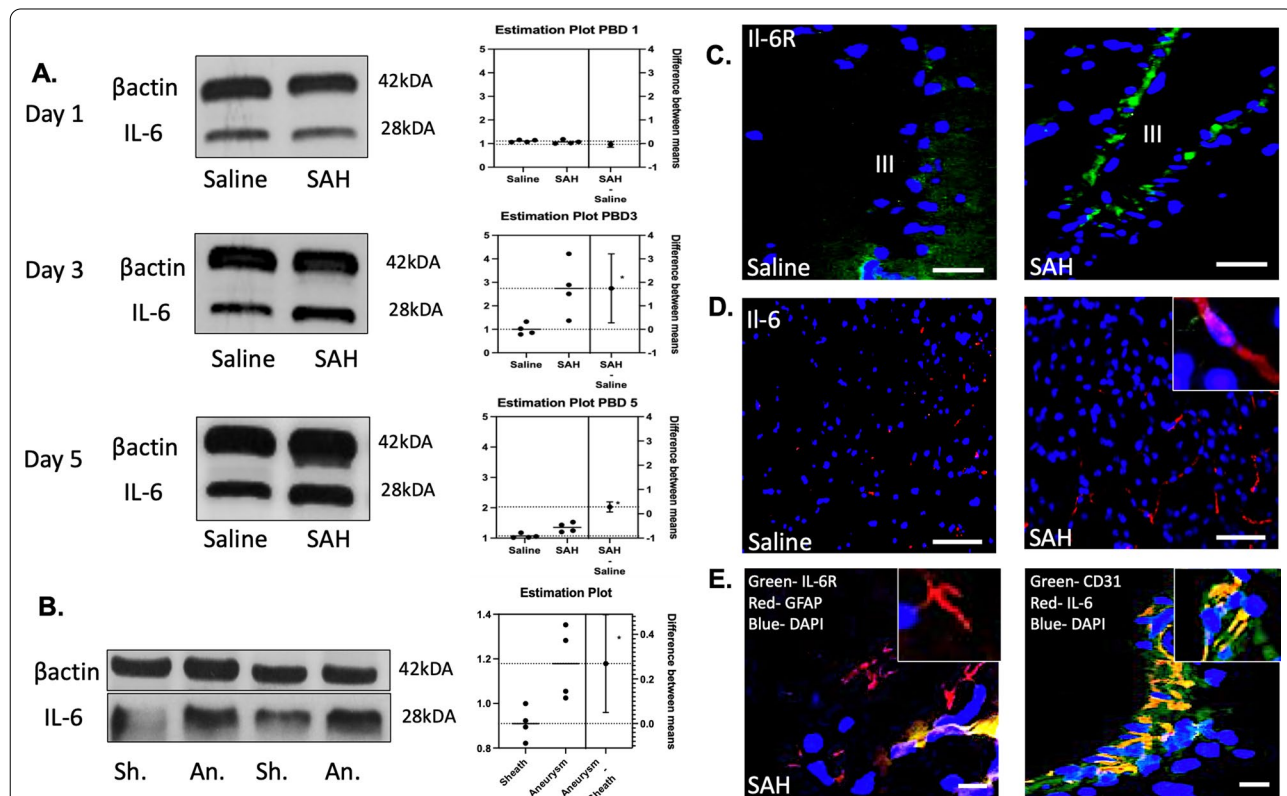
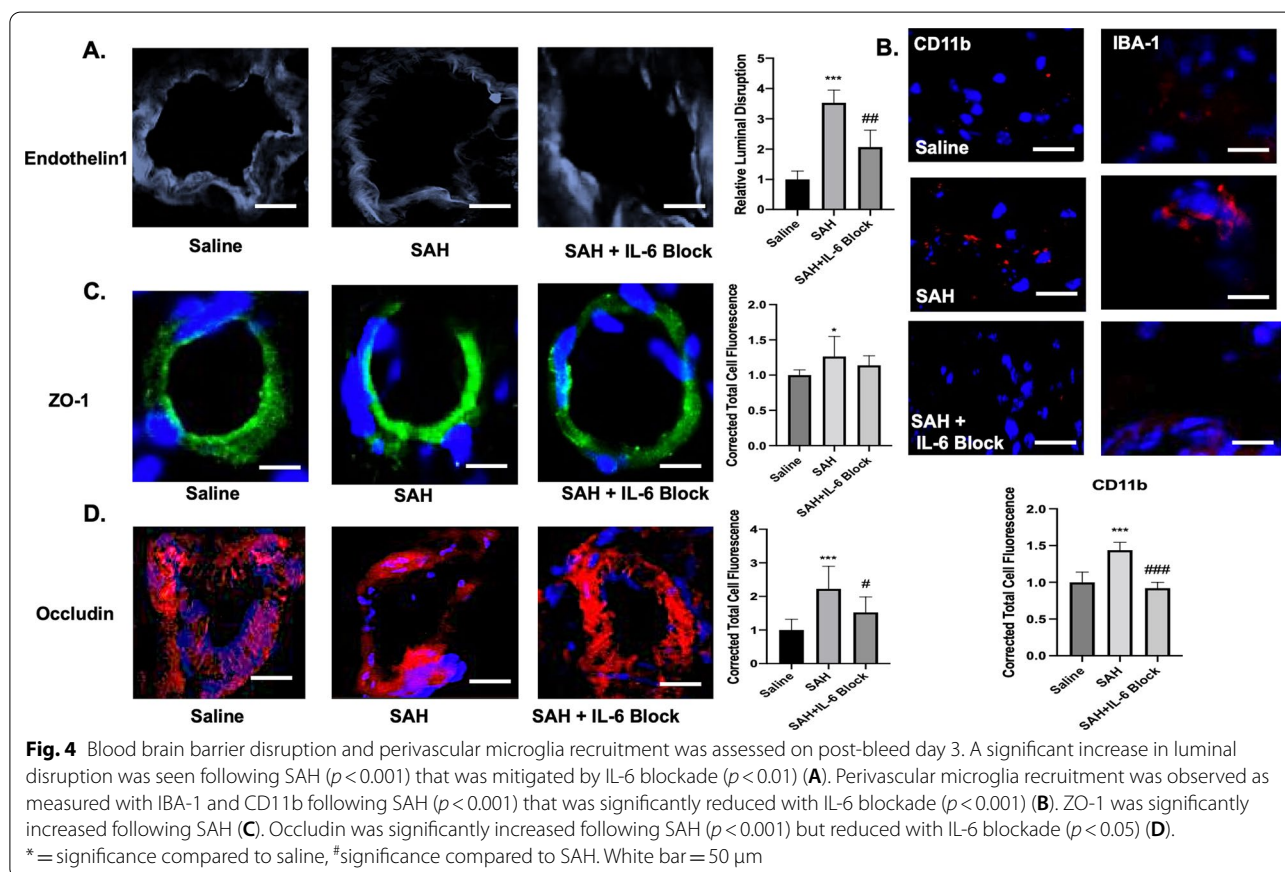
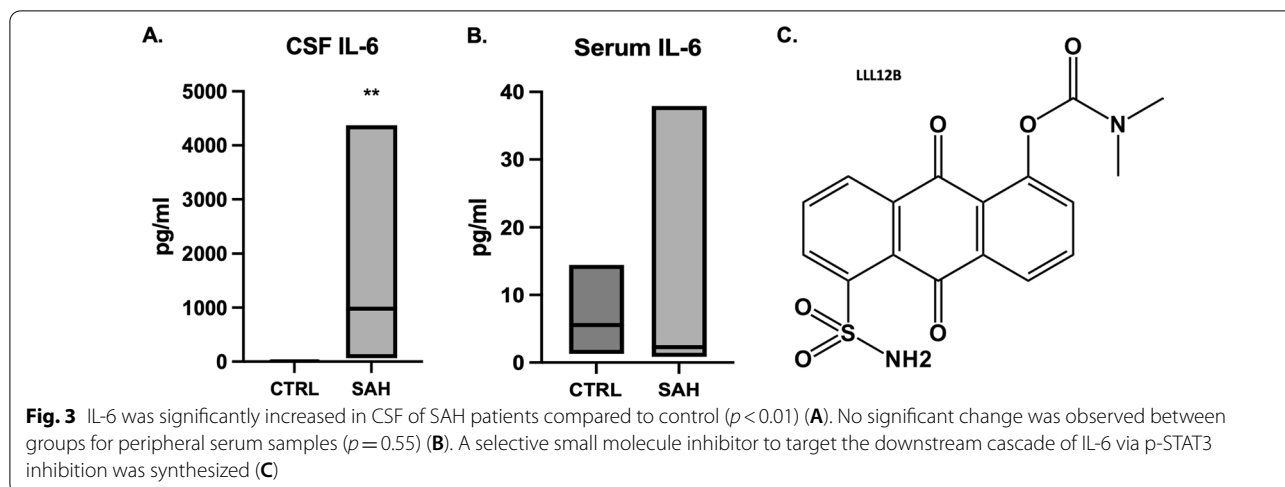


Fig. 2 IL-6 measurements in both peripheral blood and brain. A peak in IL-6 was seen on post-SAH day 3 and sustained on post-SAH day 5 ($p<0.05$) (A). IL-6 was also increased in aneurysmal blood versus sheath blood in human samples ($p<0.05$) (B). IL-6 receptor increase was seen in perivascular distribution on post-bleed day 3 (C). IL-6 release was perivascular in distribution (D). Co-localization revealed surrounding reactive astrocytes and IL-6 increased expression with endothelial markers (E). White bar panel B = 60 μ m, C = 50 μ m, panel D = 30 μ m



IL-6 blockade reduced the microglia recruitment with mean difference 0.52 between SAH vs. SAH + IL-6 block ($q = 14.7, p < 0.001$) (Fig. 4B). A significant difference was seen between groups for ZO-1 ($F(2,27) = 4.96, p = 0.14$). A mean difference of 0.26 was seen between saline vs. SAH ($q = 4.45, p = 0.01$). No significant difference was

seen with IL-6 blockade (Fig. 4C). A significant difference was seen between groups for occludin (IL-6 blockade provided significant benefit in preserving occludin ($F(2,26) = 13.75, p < 0.001$). A mean difference of 1.23 was seen between saline vs. SAH ($q = 7.37, p < 0.001$). IL-6 blockade prevented occludin dysregulation with

mean difference 0.7 between SAH vs. SAH + IL-6 block ($q=4.32, p=0.014$) (Fig. 4D).

IL-6 knockout protects against vasospasm, secondary cascades, and reduction of cerebral blood flow following subarachnoid hemorrhage

A significant difference between groups was seen for knockout mice on post-SAH day 5 ($F(2,12)=8.85, p=0.004$). IL-6 knockout mice displayed no evidence of vasospasm compared to saline. When systemic IL-6 was given to the knockout mice immediately prior and after SAH, vasospasm resulted compared to saline with a mean difference 0.15 ($q=5.291, p=0.007$) (Fig. 5A). To investigate downstream mechanisms, p-STAT3 western blot was utilized and revealed a significant difference between groups ($F(2,9)=118.5, p<0.001$). Post hoc analysis revealed mean difference 0.3 between saline vs. SAH KO ($q=7.77, p=0.008$), mean difference 0.47 between saline vs. SAH KO with endogenous IL-6 administration ($q=21.5, p<0.001$), and mean difference 0.169 between SAH KO and SAH KO with endogenous

IL-6 administration ($q=13.73, p=0.002$). p-STAT3 was co-localized with TLR4 in a similar perivascular distribution for the SAH KO with endogenous IL-6 administration compared to SAH wild type (Fig. 5B). A significant difference in blood flow was seen between groups ($F(3,12)=15.42, p<0.001$). A reduction in right MCA cerebral blood flow was seen for SAH mice vs. saline with mean difference 0.19 ($q=9.49, p<0.001$). This was mitigated by IL-6 blockade vs. SAH with mean difference 0.12 ($q=6.04, p=0.005$), and IL-6 KO vs. SAH with mean difference 0.09 ($q=4.75, p=0.026$) (Fig. 5C).

Peripheral macrophages enter post-SAH day 5; IL-6 blockade blunts caveolin increase

In regions of vasospasm, it was noted that peripheral myeloid cells (macrophages) infiltrated adjacent to regions of microglia activation (Fig. 6A). This was seen along the MCA distribution internal to where the SAH blood was noted. The myeloid infiltration was not seen in regions that were not associated with vasospasm. A significant increase in IL-6 receptors was associated in

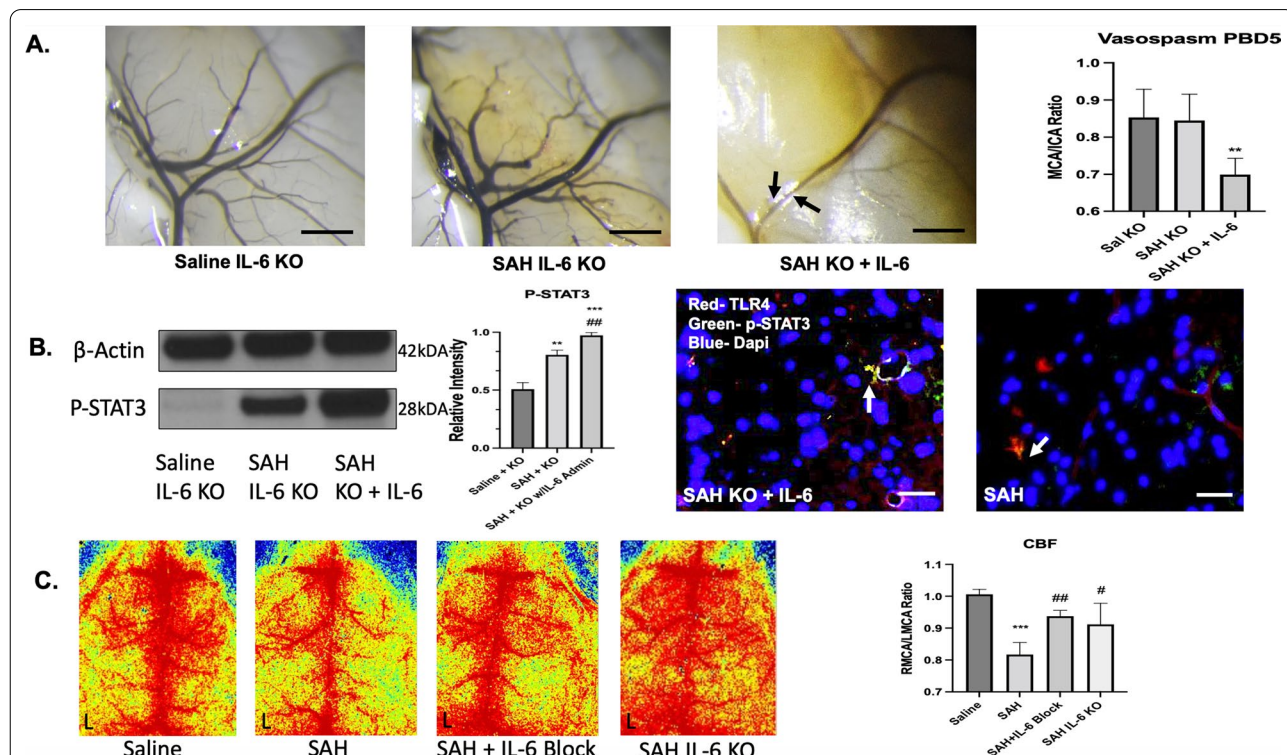
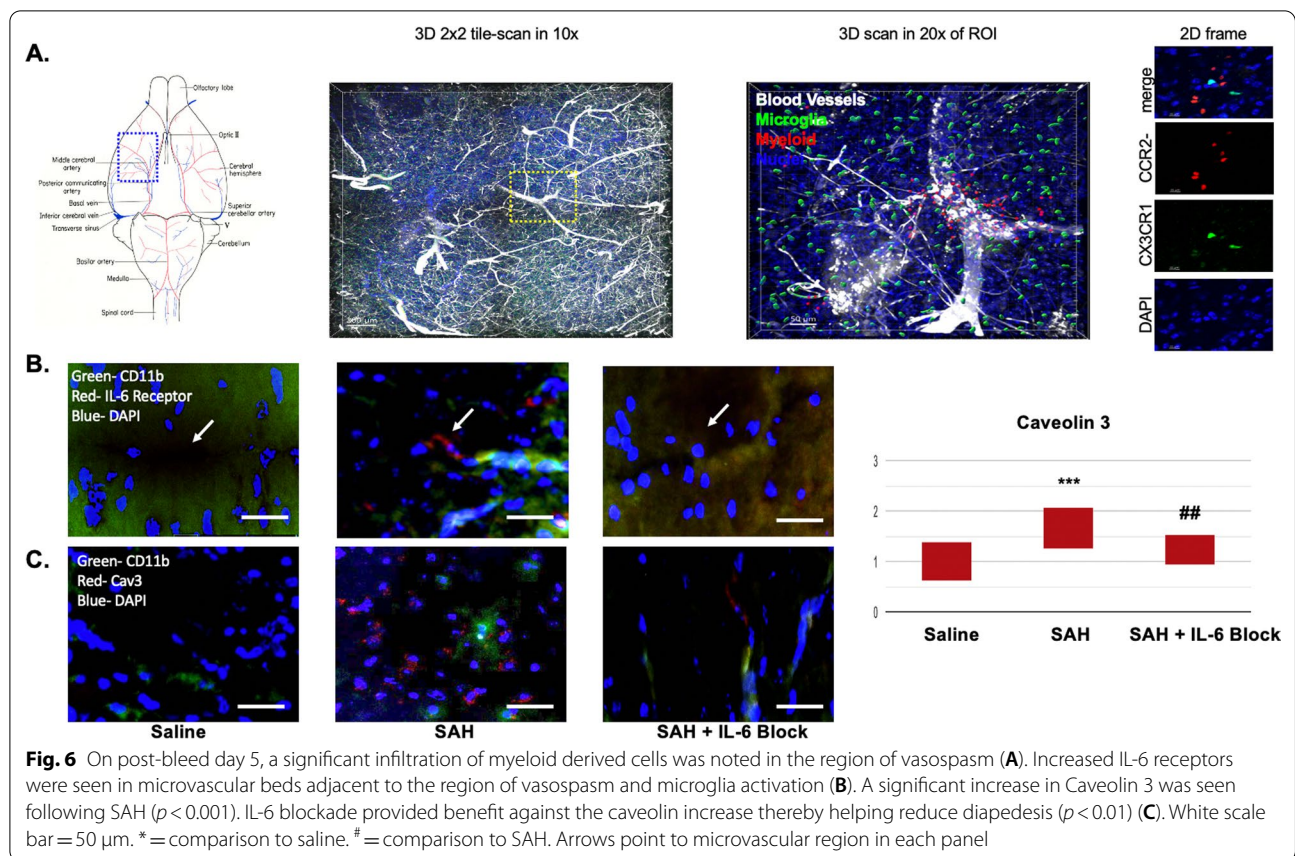


Fig. 5 IL-6 knockout is protective against decreased cerebral blood flow, vasospasm, and secondary cascades. On post-bleed day 5, no significant increase in vasospasm was seen in the SAH IL-6 KO group. When IL-6 was administered to the knockout mice in context of SAH, vasospasm developed ($p<0.01$) (A). IL-6 administration to the SAH KO mice significantly increased p-STAT3 compared to saline ($p<0.001$) and to SAH IL-6 KO without administration ($p<0.01$). p-STAT3 and TLR4 co-localization was similar between the SAH IL-6 KO mice with IL-6 administration and SAH wild-type mice (B). A significant decrease in RMCA/LMCA ratio cerebral blood flow was seen 48 h after SAH $p<0.001$. This was partially mitigated by IL-6 blockade ($p<0.01$) and IL-6 KO ($p<0.05$) (C). Black scale bare = 100 μ m. White scale bar = 50 μ m. *comparison to saline. #b = comparison to SAH + KO. #c = comparison to SAH



microvasculature surrounding the region of vasospasm and adjacent to activated microglia (Fig. 6B). These same regions had a significant increase in caveolin 3 (Fig. 6C). A significant difference between groups was noted ($F(2,57) = 15.64, p < 0.001$). Post hoc analysis revealed a significant difference between saline (mean 1) and SAH (mean 1.65) ($p < 0.001$). IL-6 blockade provided protective benefit against SAH (mean 1.23) ($p < 0.01$).

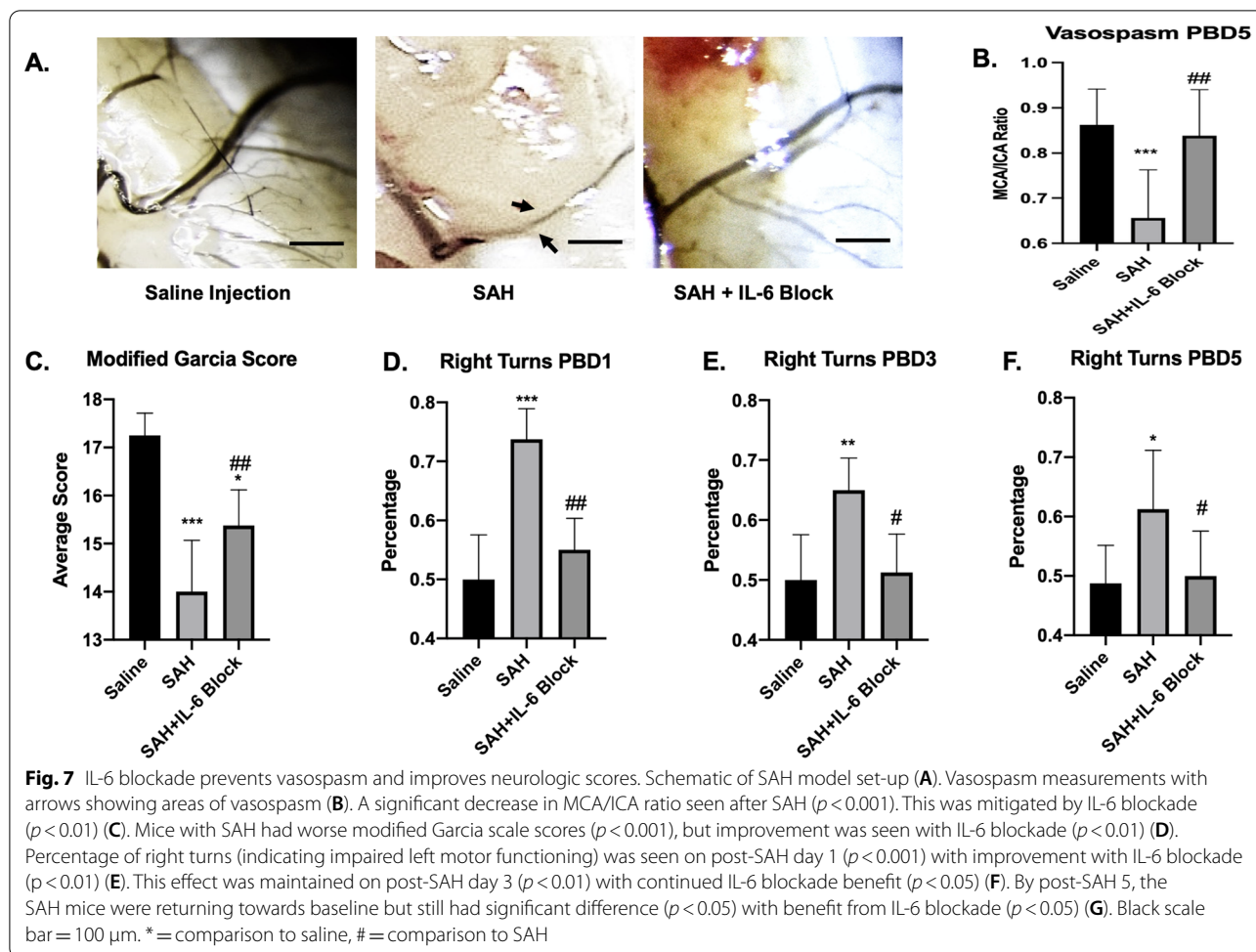
Pharmacologic IL-6 blockade prevents vasospasm and improves neurologic performance

Significant difference between groups was seen for vasospasm post-SAH day 5 ($F(2,24) = 11.44, p < 0.001$). Vasospasm was noted between saline versus SAH with mean difference 0.21 ($q = 6.28, p < 0.001$). IL-6 blockade mitigated this effect with mean difference versus SAH 0.19 ($q = 5.39, p = 0.003$) (Fig. 7A, B). A significant difference was also noted between groups for modified Garcia scores ($F(2,21) = 33.43, p < 0.001$). SAH mice has worse scores compared to saline (14 vs. 17.25 with $q = 11.52, p < 0.001$) IL-6 blockade provided some protective benefit versus SAH (mean difference 1.38, $p = 0.007$) (Fig. 7C). A significant difference between groups was seen for the right turn test post-SAH day 1 ($F(2,21) = 33.44, p < 0.001$),

post-SAH day 3 ($F(2,21) = 13.11, p < 0.001$, and post-SAH day 5 ($F(2,21) = 5.79, p < 0.01$). SAH mice spent 74% turning to right (indicating left sided deficits) on day 1 compared to 50% for saline and 55% for IL-6 blockade (saline vs. SAH $q = 10.97, p < 0.001$; SAH vs. SAH + IL-6 blockade $q = 8.66, p < 0.01$). On day 3 SAH mice spent 65% turning to right compared to 50% for saline and 51% for IL-6 blockade (saline vs. SAH $q = 6.52, p < 0.01$; SAH vs. SAH + IL-6 blockade $q = 5.9, p < 0.05$). On day 5, SAH mice spent 61% turning right compared to 48% saline and 50% IL-6 blockade (saline vs. SAH $q = 4.37, p = 0.015$; SAH vs. SAH + IL-6 blockade $q = 3.93, p = 0.03$) (Fig. 7D–F).

Subarachnoid hemorrhage induces microglia alteration

On PBD5, SAH induced microglia phenotype switching. CD11b was co-localized with COX2, Arg1, and iNOS. Overlap coefficients with CD11b and COX2 for saline $r = 0.78$ ($k1 0.73, k2 1.24$), SAH $r = 0.65$ ($k1 0.55, k2 1.45$), and SAH + IL-6 blockade $r = 0.81$ ($k1 0.76, k2 1.19$) (Fig. 8A). Overlap coefficients with CD11b and Arg1 for saline $r = 0.77$ ($k1 0.75, k2 1.28$), SAH $r = 0.96$ ($k1 0.93, k2 1.055$), and SAH + IL-6 blockade $r = 0.96$ ($k1 0.81, k2 1.21$) (Fig. 8B). Overlap coefficients with CD11b and



iNOS for saline $r = 0.86$ (k_1 0.84, k_2 1.078), SAH $r = 0.94$ (k_1 0.85, k_2 1.147), and SAH + IL-6 blockade $r = 0.66$ (k_1 0.63, k_2 1.6) (Fig. 8C).

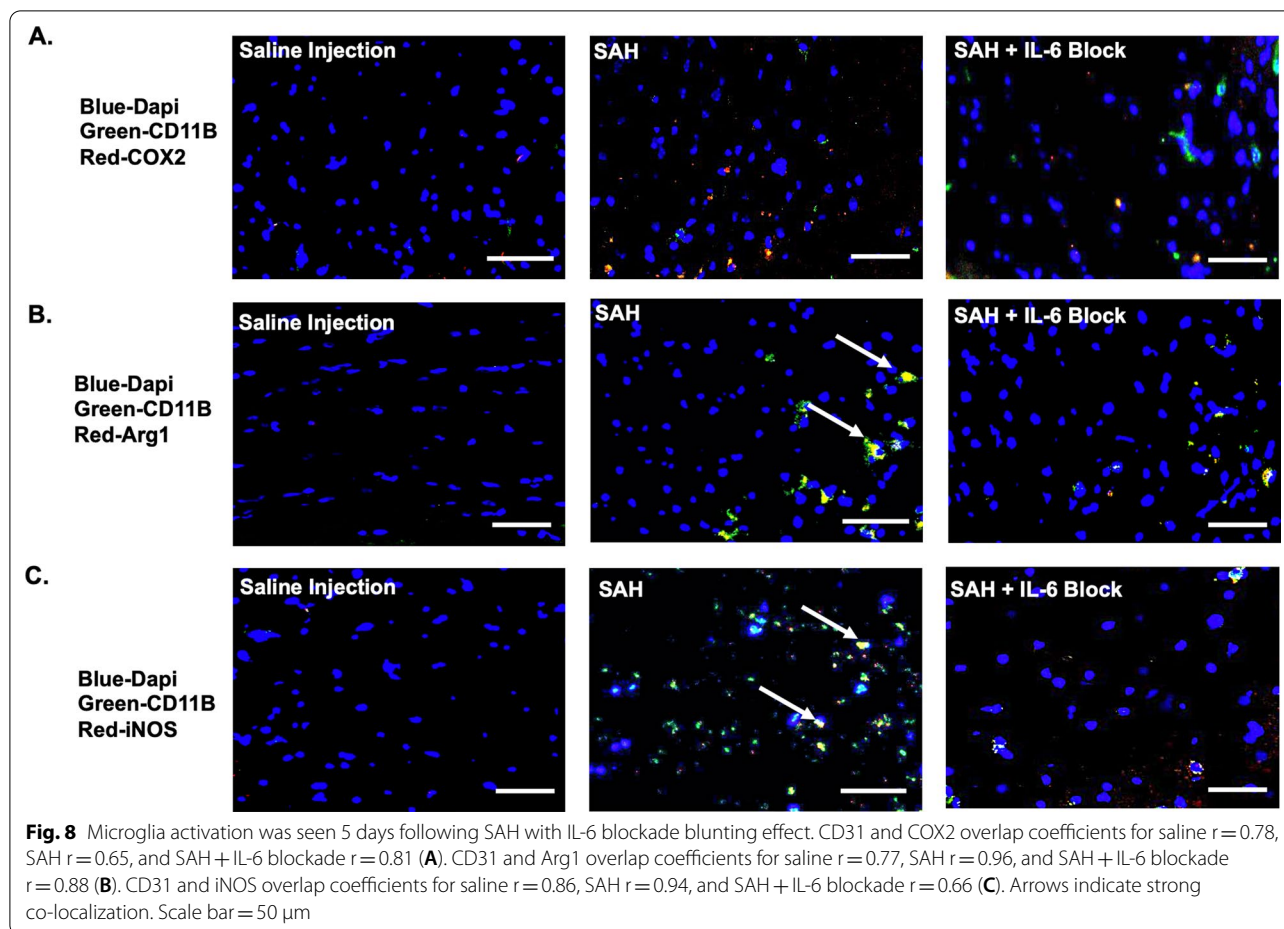
Subarachnoid hemorrhage initiates downstream cascades that are alleviated by IL-6 blockade

Toll-like receptor 4 (TLR4) expression was significantly different between groups 7 days following SAH ($F(2,15)$ 89.54, $p < 0.001$). Post hoc comparison showed a mean difference of 15.83 for SAH versus saline ($q = 18.83$, $p < 0.001$). This effect was significantly reduced with IL-6 blockade versus SAH with mean difference 9.333 ($q = 11.1$, $p < 0.01$) (Fig. 9A). P-STAT3 was also significantly different between groups ($F(2,27)$ 132, $p < 0.001$). A significant mean difference of 13.5 was seen between SAH versus saline ($q = 22.81$, $p < 0.001$). IL-6 blockade significantly reduced this effect with mean difference 8.2 versus SAH ($q = 13.85$, $p < 0.01$) (Fig. 9B). Caspase 3 was significantly different between groups following SAH ($F(2,27)$ 49.45, $p < 0.001$). A mean difference of 0.6898 was seen between SAH versus saline ($q = 13.61$ $p < 0.001$).

IL-6 blockade mitigated the increased caspase 3 activation with mean difference 0.5 versus SAH ($q = 9.86$, $p < 0.01$) (Fig. 9C).

Selective p-STAT3 inhibition shows protective benefit of targeting IL-6 pathway

NFKB expression was significantly different between groups 7 days following SAH ($F(2,147)$ 19.54, $p < 0.001$). Post hoc comparison showed a mean difference of 1.45 for SAH versus saline ($q = 8.07$, $p < 0.001$). This effect was significantly reduced with p-STAT3 blockade versus SAH with mean difference 1.29 ($q = 7.17$, $p < 0.001$) (Fig. 10A). Toll-like receptor 4 (TLR4) expression was significantly different between groups 7 days following SAH ($F(2,147)$ 31.4, $p < 0.001$). Post hoc comparison showed a mean difference of 1.26 for SAH versus saline ($q = 9.36$, $p < 0.001$). This effect was significantly reduced with p-STAT3 blockade versus SAH with mean difference 1.35 ($q = 10.02$, $p < 0.01$) (Fig. 10B). Nitrotyrosine was significantly different between groups following SAH ($F(2,57)$ 281.9, $p < 0.001$). A mean difference of 15.75 was



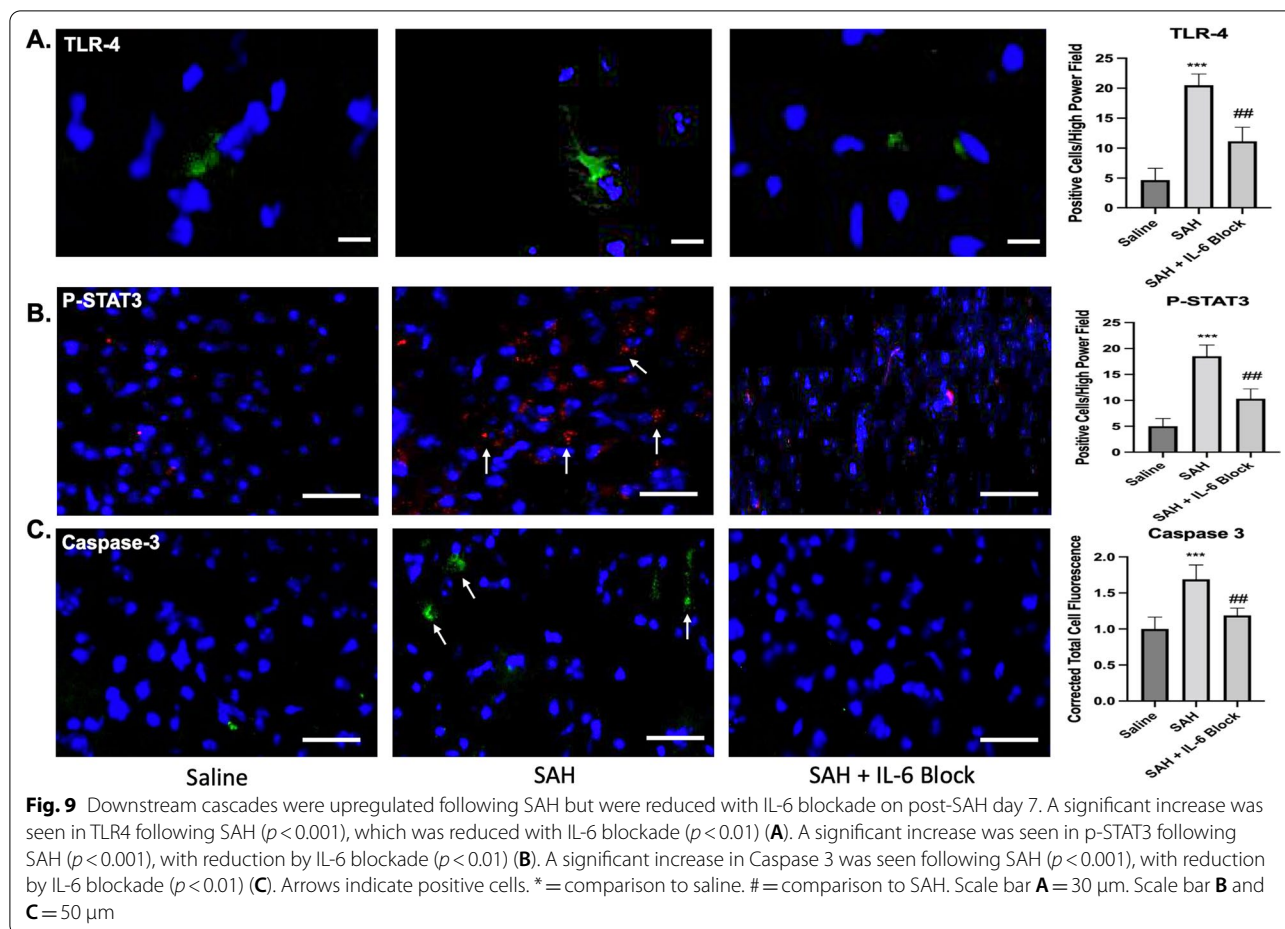
seen between SAH versus saline ($q = 33.02$, $p < 0.001$). P-STAT3 blockade mitigated the increased nitrotyrosine activity with mean difference 10.4 versus SAH ($q = 21.8$, $p < 0.001$), but did not completely abolish it compared to control ($p < 0.05$) (Fig. 10C).

Targeting IL-6 provided protection against ventriculomegaly and cell death

SAH furthermore induced increased 3rd ventricle diameter on day 9 with a significant difference between groups ($F(2, 15) = 36.65$, $p < 0.001$). A mean difference of 0.12 was seen between saline versus SAH ($q = 11.76$, $p < 0.01$). IL-6 blockade prevented the ventriculomegaly consistent with hydrocephalus when compared to SAH with mean difference 0.09 ($q = 8.38$, $p < 0.05$) (Fig. 11A). SAH also induced cell death as measured with TUNEL staining with a significant difference between groups ($F(2,15) = 277.6$, $p < 0.001$). A mean difference between saline versus SAH was 31.17 ($q = 33.3$, $p < 0.001$). This cell death was drastically reduced with IL-6 blockade with mean difference 14.67 ($q = 15.67$, $p < 0.05$) (Fig. 11B).

Discussion

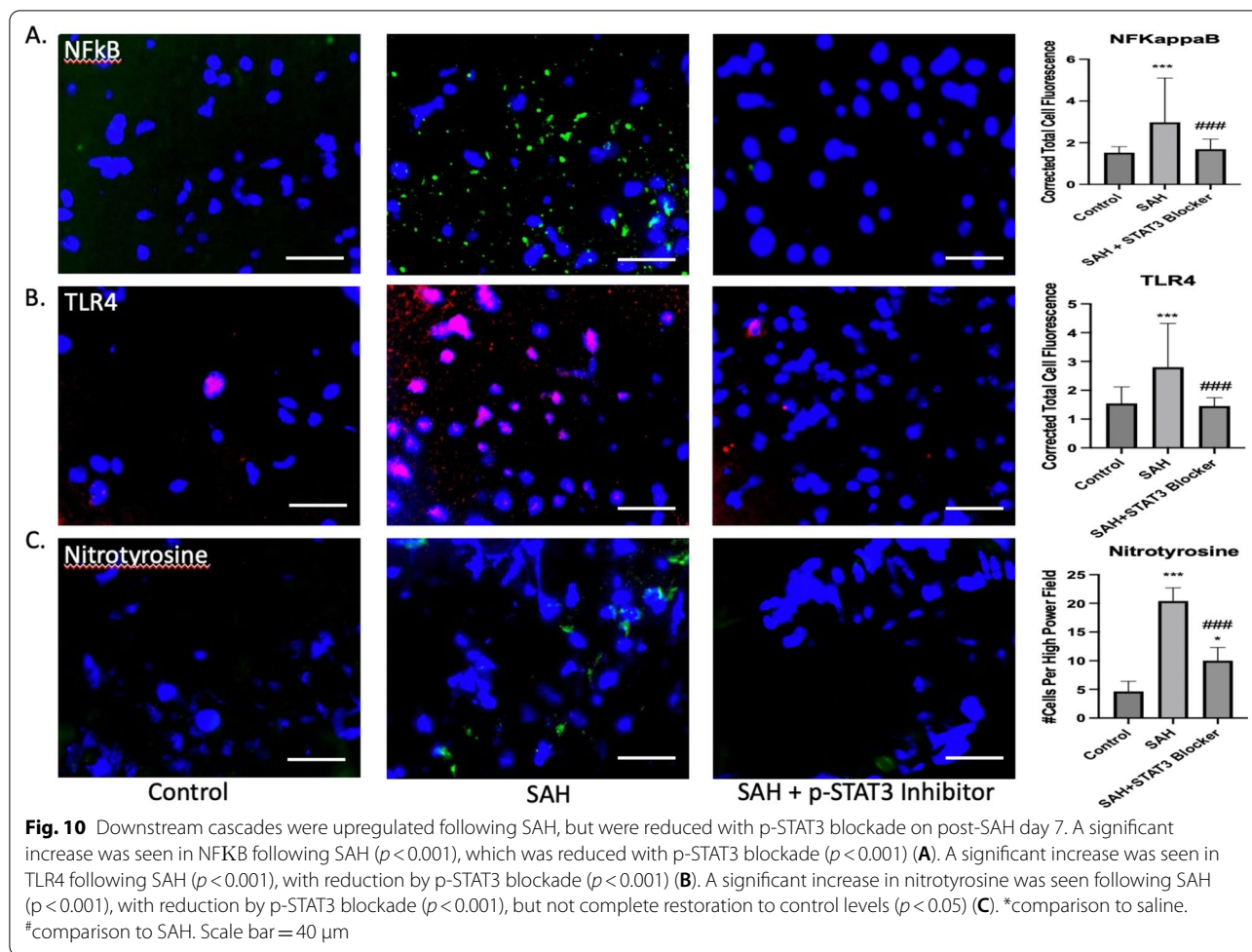
IL-6 has been shown clinically to peak on day 3 following SAH and is a reliable marker for vasospasm [25]. Despite strong evidence of correlation, limited work has been done regarding mechanistic contribution [26]. In this paper, we sought to investigate the mechanistic contribution following SAH through use of IL-6 blockade, IL-6 systemic KO, and STAT3 inhibition. A peak of IL-6 was seen on post-SAH day 3 and upon further assessment distribution within the brain was both periventricular and perivascular. Likewise, the human aneurysmal blood had significant increase in IL-6 compared to sheath blood. A significant increase in CSF IL-6 was seen compared to controls correlating to clinical relevance. Other groups have shown that reactive astrocytes and microglia release IL-6 at the endothelial interface following neural injury [27]. We also found a release at the endothelial interface adjacent to reactive astrocytes. This was associated with an increase in Caveolin 3. Caveolin 3 prepares the BBB for diapedesis of peripheral macrophages. Baduati and colleagues propose a complex interplay between astrocytes and microglia to facilitate this process [28]. It



has been postulated that the release of IL-6 and increased caveolin facilitates BBB breakdown via an inflammatory-dependent response and downstream activation of TLR4 and p-STAT3 pathway mediated via microglia [29]. Not surprisingly, we found an increase in tight junction protein disruption and luminal irregularity consistent with BBB breakdown on post-SAH day 3. Importantly, we noticed a sharp increase in activated microglia in a perivascular distribution at this same time point, indicating early recruitment as the inflammatory surge rises. This increase was associated with recruitment and infiltration of peripheral myeloid cells. We found that IL-6 blockade prevented BBB disruption and perivascular microglia recruitment on post-SAH day 3 by reducing the pro-inflammatory state. IL-6 blockade also reduced the caveolin increase, thereby stopping the inflammatory recruitment.

Emerging evidence has linked dysregulation of CBF as a contributor to the early BBB breakdown and induction of neuroinflammation [30]. To further test the importance of cerebral autoregulatory perfusion, we measured CBF at 48 h. A significant disruption in right MCA perfusion

was seen following SAH. IL-6 KO, and IL-6 blockade prevented this flow disruption through reduced activation of the inflammatory cascade. Maddahi and colleagues noted decreased perfusion 48 h post-SAH in their model and highlighted the correlation with the beginning of the IL-6 surge [31]. Autoregulatory dysfunction may therefore be a key contributor to the early BBB breakdown and inflammatory surge. It likely indicates one of the protective roles we observed with IL-6 blockade and noted benefit of reducing microglia recruitment early. The next logical progression was to look to vasospasm. In our mouse model, we found a vasospasm peak on post-SAH day 5. Both IL-6 blockade and KO prevented the vasospasm development. When IL-6 was reintroduced to the KO mice in the context of SAH, they developed vasospasm in a similar manner to wild-type SAH mice. To tease apart the mechanism, we investigated downstream cascades with specific emphasis on the downstream consequences of the inflammatory cascade. Suzuki and colleagues reported that the TLR4/STAT3 pathway is integral to vasospasm development [32]. The proposed mechanism is a positive feedback loop with IL-6 and may

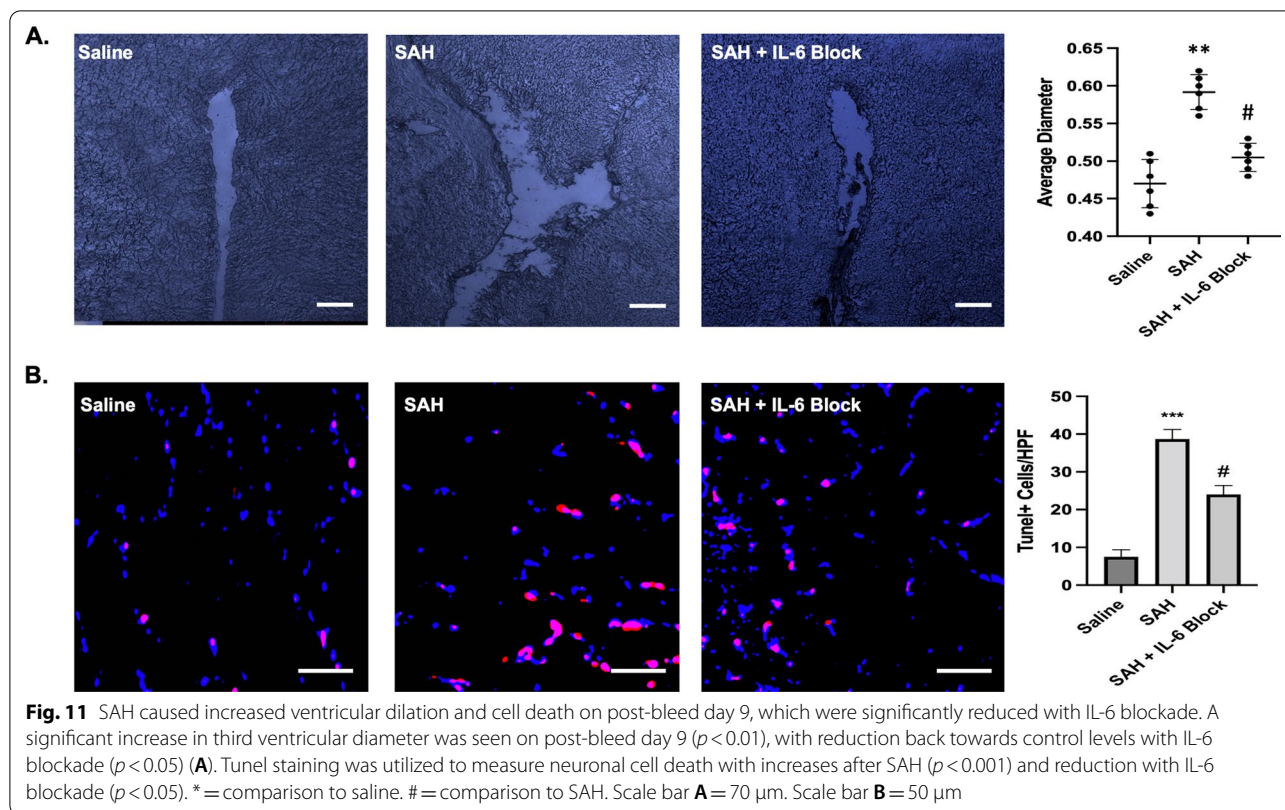


account for the sustained IL-6 levels we found on post-SAH day 5. The graphical abstract shows how IL-6 blockade targets both phases of the IL-6 response.

In our model, we found that IL-6 KO reduced p-STAT3 and TLR4 on post-SAH day 5. This was likely due to a unique microglia phenotype switch, which was prevented by IL-6 blockade. We further selectively targeted p-STAT3 to confirm importance of pathway and found protective benefit against neuroinflammation and oxidative stress. Further projects will help elucidate the role of peripheral macrophages in inducing this switch. We have shown here the early infiltration of peripheral myeloid cells. IL-6 blockade provided similar protective benefit to that seen by IL-6 KO. In addition to reduced vasospasm, the mice with IL-6 blockade had improved modified Garcia scale scores and turn test performance compared to SAH counterparts. Neuroprotection following SAH consists not only of vasospasm treatment, but also prevention of delayed cerebral ischemia (DCI). IL-6 blockade prevented activation of the apoptotic pathway on post-SAH day 7. More selective targeting via the p-STAT3

inhibition confirmed this mechanistic significance. Furthermore, it reduced cell death as measured with TUNEL staining on post-SAH day 9. An interesting correlation has been postulated regarding IL-6 surge, vasospasm, and hydrocephalus requiring shunting [33]. We found that IL-6 blockade prevented the increased diameter of the 3rd ventricle after SAH. Again, the inflammatory surge can cause scarring at the arachnoid granulations, which is not present if early inflammatory recruitment is halted. Microglia activation has been associated with both vasospasm and hydrocephalus and is closely regulated by the IL-6 pathway and NLRP3 inflammasome [34].

We had previously reported benefit of NLRP3 inhibition following SAH. In this paper, we found that IL-6 blockade had significant regulation on another arm of the inflammatory spectrum starting on post-SAH day 3 and extending to day 5. Hanafy found that TLR4 knockout in microglia had significant benefit on reducing vasospasm [35]. Likewise reducing IL-6 mitigated the TLR4 response in our model. We have shown that this response is mechanistically linked to the IL-6 surge and



that by targeting this surge significant neuroprotective benefit is achieved in a novel mechanistic manner. An area of ongoing investigation is the microglia/peripheral immune crosstalk, which is a topic for future studies. A primary limitation of the study is lack of cerebrospinal fluid collection at extended dates to correlate with timing of delayed cerebral ischemia. Ongoing collaborations are underway to investigate this important human mechanistic time sequence.

Conclusion

Mechanistic studies regarding the role that IL-6 plays in vasospasm development had up to this point been lacking. Utilizing a host of different assays, inhibition, and knockout animals, we have teased apart the beginning of a mechanistic pathway via the inflammation cascade mediated via STAT3 and peripheral macrophage infiltration. Ongoing work is needed regarding the crosstalk between microglia and peripheral immune cells, which will improve understanding and aid in advancement to first in human trials.

Abbreviations

BBB: Blood brain barrier; CBF: Cerebral blood flow; CV: Cerebral vasospasm; DCI: Delayed cerebral ischemia; IL-6: Interleukin-6; ICA: Internal cerebral artery; KO: Knock out; MCA: Middle cerebral artery; NLRP3: NLR family pyrin domain

containing 3; RIPA: Radio-immunoprecipitation assay; STAT3: Signal transducer and activator of transcription 3 ; SAH: Subarachnoid hemorrhage; TLR4: Toll-like receptor 4.

Acknowledgements

We thank the Harrison laboratory for assistance with providing the dual labeled animals.

Author contributions

BL formulated project, conducted experiments, wrote paper. WD assisted with experiments and critical editing. KM critical editing, KH expert feedback, DL critical editing, MM experimental assistance, VD experimental assistance, CV assistance with clarity analysis, NC expert insight, RJ experimental assistance, BH senior scientist, project review, oversight. All authors read and approved the final manuscript.

Funding

Brandon Lucke-Wold was funded through NIH R25 grant.

Availability of data and materials

Not applicable.

Declarations

Ethics approval and consent to participate

All participants consented for participation under IRB approved consent process.

Consent for publication

All authors consent for publication.

Competing interests

The authors declare that they have no competing interests.

Author details

¹Department of Neurosurgery, University of Florida, Gainesville, FL, USA. ²Department of Physiologic Sciences, University of Florida, Gainesville, FL, USA. ³Department of Radiology, Neuroradiology Division, University of Florida, Gainesville, FL, USA. ⁴Department of Medicinal Chemistry, University of Florida, Gainesville, FL, USA.

Received: 23 May 2022 Accepted: 7 September 2022

Published online: 16 September 2022

References

- Lenski M, Hüge V, Briegel J, Tonn JC, Schichor C, Thon N. Interleukin 6 in the cerebrospinal fluid as a biomarker for onset of vasospasm and ventriculitis after severe subarachnoid hemorrhage. *World Neurosurg.* 2017;99:132–9.
- Croci D, Nevzati E, Muroi C, Schopf S, Hornemann T, Widmer HR, Danura H, Fandino J, Marbacher S. Changes in the cerebrospinal fluid lipid profile following subarachnoid hemorrhage in a closed cranium model: correlations to cerebral vasospasm, neuronal cell death and Interleukin-6 synthesis. A pilot study. *J Stroke Cerebrovasc Dis.* 2020;29(9):105054.
- Croci DM, Sivanrupan S, Wanderer S, Agnoletto GJ, Chiappini A, Gruter BE, Anderegg L, Mariani L, Taussky P, Marbacher S. Preclinical and clinical role of interleukin-6 in the development of delayed cerebral vasospasm and neuronal cell death after subarachnoid hemorrhage: towards a potential target therapy? *Neurosurg Rev.* 2021. <https://doi.org/10.1007/s10143-021-01628-9>.
- Vlachogiannis P, Hillered L, Khalil F, Enblad P, Ronne-Engstrom E. Interleukin-6 Levels in Cerebrospinal Fluid and Plasma in Patients with Severe Spontaneous Subarachnoid Hemorrhage. *World Neurosurg.* 2019;122:e612–8.
- Croci D, Nevzati E, Danura H, Schopf S, Fandino J, Marbacher S, Muroi C. The relationship between IL-6, ET-1 and cerebral vasospasm, in experimental rabbit subarachnoid hemorrhage. *J Neurosurg Sci.* 2019;63(3):245–50.
- Lucke-Wold B, Hosaka K, Dodd W, Motwani K, Laurent D, Martinez M, Hoh B. Interleukin-6: important mediator of vasospasm following subarachnoid hemorrhage. *Curr Neurovasc Res.* 2021. <https://doi.org/10.2174/1567202618666211104122408>.
- Gowrisankar YV, Clark MA. Angiotensin II induces interleukin-6 expression in astrocytes: role of reactive oxygen species and NF-kappaB. *Mol Cell Endocrinol.* 2016;437:130–41.
- Damm J, Luheshi GN, Gerstberger R, Roth J, Rummel C. Spatiotemporal nuclear factor interleukin-6 expression in the rat brain during lipopolysaccharide-induced fever is linked to sustained hypothalamic inflammatory target gene induction. *J Comp Neurol.* 2011;519(3):480–505.
- Recasens M, Almolda B, Perez-Clausell J, Campbell IL, Gonzalez B, Castellano B. Chronic exposure to IL-6 induces a desensitized phenotype of the microglia. *J Neuroinflammation.* 2021;18(1):31.
- Wang Y, Kong XQ, Wu F, Xu B, Bao DJ, Cheng CD, Wei XP, Dong YF, Niu CS. SOCS1/JAK2/STAT3 axis regulates early brain injury induced by subarachnoid hemorrhage via inflammatory responses. *Neural Regen Res.* 2021;16(12):2453–64.
- Dodd WS, Noda I, Martinez M, Hosaka K, Hoh BL. NLRP3 inhibition attenuates early brain injury and delayed cerebral vasospasm after subarachnoid hemorrhage. *J Neuroinflammation.* 2021;18(1):163.
- Marbacher S, Gruter B, Schopf S, Croci D, Nevzati E, D'Alonzo D, Lattmann J, Roth T, Bircher B, Wolfert C, et al. Systematic review of in vivo animal models of subarachnoid hemorrhage: species, standard parameters, and outcomes. *Transl Stroke Res.* 2018. <https://doi.org/10.1007/s12975-018-0657-4>.
- Cao G, Ye X, Xu Y, Yin M, Chen H, Kou J, Yu B. YiQiFuMai powder injection ameliorates blood-brain barrier dysfunction and brain edema after focal cerebral ischemia-reperfusion injury in mice. *Drug Des Devel Ther.* 2016;10:315–25.
- Tsukamoto H, Senju S, Matsumura K, Swain SL, Nishimura Y. IL-6-mediated environmental conditioning of defective Th1 differentiation dampens antitumor immune responses in old age. *Nat Commun.* 2015;6:6702.
- Vida M, Gavito AL, Pavon FJ, Bautista D, Serrano A, Suarez J, Arrabal S, Decara J, Romero-Cuevas M, Rodriguez de Fonseca F et al: Chronic administration of recombinant IL-6 upregulates lipogenic enzyme expression and aggravates high-fat-diet-induced steatosis in IL-6-deficient mice. *Dis Model Mech* 2015, 8(7):721–731.
- Li R, Ma K, Zhao H, Feng Z, Yang Y, Ge H, Zhang X, Tang J, Yin Y, Liu X, et al. Cattle encephalon glycoside and ignotin reduced white matter injury and prevented post-hemorrhagic hydrocephalus in a rat model of intracerebral hemorrhage. *Sci Rep.* 2016;6:35923.
- Bouet V, Freret T, Toutain J, Divoux D, Boulouard M, Schumann-Bard P. Sensorimotor and cognitive deficits after transient middle cerebral artery occlusion in the mouse. *Exp Neurol.* 2007;203(2):555–67.
- Logsdon AF, Lucke-Wold BP, Nguyen L, Matsumoto RR, Turner RC, Rosen CL, Huber JD. Salubrinal reduces oxidative stress, neuroinflammation and impulsive-like behavior in a rodent model of traumatic brain injury. *Brain Res.* 2016;1643:140–51.
- Logsdon AF, Lucke-Wold BP, Turner RC, Li X, Adkins CE, Mohammad AS, Huber JD, Rosen CL, Lockman PR. A mouse model of focal vascular injury induces astrocyte reactivity, tau oligomers, and aberrant behavior. *Arch Neurosci.* 2017. <https://doi.org/10.5812/archneurosci.44254>.
- Lucke-Wold BP, Logsdon AF, Turner RC, Huber JD, Rosen CL. Endoplasmic reticulum stress modulation as a target for ameliorating effects of blast induced traumatic brain injury. *J Neurotrauma.* 2017;34(S1):S62–70.
- Lucke-Wold BP, Turner RC, Logsdon AF, Nguyen L, Bailes JE, Lee JM, Robson MJ, Omalu BI, Huber JD, Rosen CL. Endoplasmic reticulum stress implicated in chronic traumatic encephalopathy. *J Neurosurg.* 2016;124(3):687–702.
- Halaoui R, Rejon C, Chatterjee SJ, Szymorski J, Meterissian S, Muller WJ, Omeroglu A, McCaffrey L. Progressive polarity loss and luminal collapse disrupt tissue organization in carcinoma. *Genes Dev.* 2017;31(15):1573–87.
- Baker KL, Daniels SB, Lenington JB, Lardaro T, Czap A, Notti RQ, Cooper O, Isacson O, Frasca S Jr, Conover JC. Neuroblast protuberances in the subventricular zone of the regenerative MRL/MpJ mouse. *J Comp Neurol.* 2006;498(6):747–61.
- Diuba AV, Samigullin DV, Kaszas A, Zonfrillo F, Malkov A, Petukhova E, Casini A, Arosio D, Esclapez M, Gross CT, et al. CLARITY analysis of the C1/pH sensor expression in the brain of transgenic mice. *Neuroscience.* 2020;439:181–94.
- Ni W, Gu YX, Song DL, Leng B, Li PL, Mao Y. The relationship between IL-6 in CSF and occurrence of vasospasm after subarachnoid hemorrhage. *Acta Neurochir Suppl.* 2011;110(Pt 1):203–8.
- Liu Z, Li Q, Cui G, Zhu G, Tang W, Zhao H, Zhang JH, Chen Y, Feng H. Blood-filled cerebrospinal fluid-enhanced pericyte microvasculature contraction in rat retina: a novel in vitro study of subarachnoid hemorrhage. *Exp Ther Med.* 2016;12(4):2411–6.
- Abbott NJ. Astrocyte-endothelial interactions and blood-brain barrier permeability. *J Anat.* 2002;200(6):629–38.
- Badaut J, Ajao DO, Sorensen DW, Fukuda AM, Pellerin L. Caveolin expression changes in the neurovascular unit after juvenile traumatic brain injury: signs of blood-brain barrier healing? *Neuroscience.* 2015;285:215–26.
- Kempuraj D, Thangavel R, Natteru PA, Selvakumar GP, Saeed D, Zahoor H, Zaheer S, Iyer SS, Zaheer A. Neuroinflammation Induces Neurodegeneration. *J Neurol Neurosurg Spine.* 2016. <https://doi.org/10.1186/s40035-020-00221-2>.
- Al-Mufti F, Amuluru K, Changa A, Lander M, Patel N, Wajswol E, Al-Marsoumi S, Alzubaidi B, Singh IP, Nuoman R, et al. Traumatic brain injury and intracranial hemorrhage-induced cerebral vasospasm: a systematic review. *Neurosurg Focus.* 2017;43(5):E14.
- Maddahi A, Ansar S, Chen Q, Edvinsson L. Blockade of the MEK/ERK pathway with a raf inhibitor prevents activation of pro-inflammatory mediators in cerebral arteries and reduction in cerebral blood flow after subarachnoid hemorrhage in a rat model. *J Cereb Blood Flow Metab.* 2011;31(1):144–54.
- Suzuki H, Fujimoto M, Kawakita F, Liu L, Nakano F, Nishikawa H, Okada T, Imanaka-Yoshida K, Yoshida T, Shiba M. Toll-like receptor 4 and tenascin-c signaling in cerebral vasospasm and brain injuries after subarachnoid hemorrhage. *Acta Neurochir Suppl.* 2020;127:91–6.
- Chaudhry SR, Stoffel-Wagner B, Kinfe TM, Guresir E, Vatter H, Dietrich D, Lamprecht A, Muhammad S. Elevated systemic IL-6 levels in patients with aneurysmal subarachnoid hemorrhage is an unspecific marker for

post-SAH complications. *Int J Mol Sci.* 2017. <https://doi.org/10.3390/ijms18122580>.

34. Zhu J, Lee MJ, Chang HJ, Ju X, Cui J, Lee YL, Go D, Chung W, Oh E, Heo JY. Reactive microglia and mitochondrial unfolded protein response following ventriculomegaly and behavior defects in kaolin-induced hydrocephalus. *BMB Rep.* 2021. <https://doi.org/10.5483/BMBRep.2022.55.4.126>.
35. Hanafy KA. The role of microglia and the TLR4 pathway in neuronal apoptosis and vasospasm after subarachnoid hemorrhage. *J Neuroinflammation.* 2013;10:83.

Publisher's Note

Springer Nature remains neutral with regard to jurisdictional claims in published maps and institutional affiliations.

Ready to submit your research? Choose BMC and benefit from:

- fast, convenient online submission
- thorough peer review by experienced researchers in your field
- rapid publication on acceptance
- support for research data, including large and complex data types
- gold Open Access which fosters wider collaboration and increased citations
- maximum visibility for your research: over 100M website views per year

At BMC, research is always in progress.

Learn more biomedcentral.com/submissions

